Bioconjugate Chemistry

Article

pubs.acs.org/bc

Intracellular Assembly of Nuclear-Targeted Gold Nanosphere Enables Selective Plasmonic Photothermal Therapy of Cancer by Shifting Their Absorption Wavelength toward Near-Infrared Region

Sajanlal R. Panikkanvalappil, Nasrin Hooshmand, and Mostafa A. El-Sayed*

Laser Dynamics Laboratory, School of Chemistry and Biochemistry, Georgia Institute of Technology, Atlanta, Georgia 30332, United States

Supporting Information

ABSTRACT: Despite the important applications of near-infrared (NIR) absorbing nanomaterials in plasmonic photothermal therapy (PPT), their high yield synthesis and nonspecific heating during the active- and passive-targeted cancer therapeutic strategies remain challenging. In the present work, we systematically demonstrate that in situ aggregation of typical non-NIR absorbing plasmonic nanoparticles at the nuclear region of the cells could translate them into an effective NIR photoabsorber in plasmonic photothermal therapy of cancer due to a significant shift of the plasmonic absorption band to the NIR region. We evaluated the potential of nuclear-targeted AuNSs as photoabsorber at various stages of endocytosis by virtue of their inherent in situ assembling capabilities at the nuclear region of the cells, which has been considered as one of the most thermolabile structures within the cells, to selectively destruct cancer cells with minimal damage to healthy cells. Various plasmonic nanoparticles such as rods and cubes have been exploited to elucidate the role of plasmonic field coupling in assembled nanoparticles and their subsequent killing efficiency. The NIR absorbing capabilities of aggregated AuNSs have been further demonstrated both experimentally and theoretically using discrete dipolar approximation (DDA) techniques, which was in concordance with the observed results in plasmonic photothermal therapeutic studies. While the current work was able to demonstrate the utility of non-NIR absorbing plasmonic nanoparticles as a potential alternative for plasmonic photothermal therapy by inducing localized plasmonic heating at the nuclear region of the cells, these findings could potentially open up new possibilities in developing more efficient nanoparticles for efficient cancer treatment modalities.

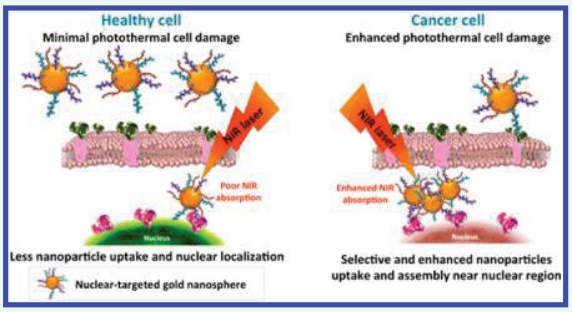

INTRODUCTION

Plasmonic photothermal therapy (PPT) is considered to be one of the promising applications of plasmonic nanoparticles in cancer treatment.[1−3] Recent advances in nanotechnology have significantly improved the efficiency of this technique by developing novel nanomaterials with high photothermal conversion efficiency and biocompatibility, which can be utilized to selectively destroy cancer cells with minimal invasiveness to the normal cells.[4,5] In PPT, cancer cell destruction is made possible by the selective and localized heating effect of the nanoparticles as a result of the enhanced local absorption of the laser radiation by the plasmonic nanoparticles.[6,7] Development of established synthetic approaches to produce nanoparticles with tunable localized surface plasmon absorption of light in the near-infrared (NIR) region further enhanced the possibilities of PPT in cancer therapeutics.[4,7−10]

Gold nanoparticles with different shapes such as rods,[1] prisms,[11] cages,[12] stars,[13] shells,[2] etc. have been widely exploited in minimally invasive cancer therapy owing to their strong absorption as well as the very high extinction coefficient at low energy NIR windows at which biological materials and tissues are relatively transparent.[1] Generally, tumor-targeting techniques utilize active or passive targeting strategies.[14] While the enhanced permeation and retention (EPR) effect[15] results in the passive accumulation of gold nanoparticles within the tumor during passive targeting, surface functionalization of nanoparticles with peptides, antibodies, etc. allows increased cellular targeting and retention during active targeting.[16] Despite important applications of NIR absorbing nanoparticles in plasmonic photothermal therapy, nonspecific heating of these NIR absorbing nanomaterials administered during active and passive targeting techniques remains a challenge as it can cause heat-induced cell death of healthy tissues. This is largely due to the fact that the NIR absorbing nanomaterials administrated during both active and passive targeted therapeutic approaches do not accumulate completely at the tumor sites. A fraction of nanoparticles will remain in the surrounding tissue environment and likely be internalized by healthy cells, which results in nonspecific heating and their ablation. Moreover, the complex synthetic procedure makes it relatively difficult to prepare such NIR absorbing nanoparticles

Received: July 21, 2017
Revised: August 21, 2017
Published: August 24, 2017

DOI: 10.1021/acs.bioconjchem.7b00427
Bioconjugate Chem. 2017, 28, 2452−2460

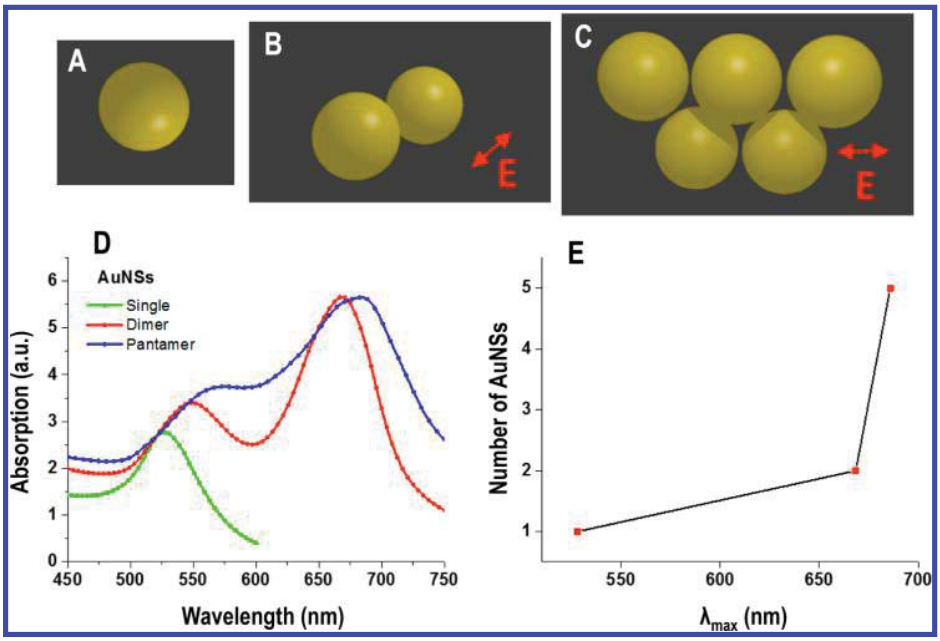

Figure 1. Pictorial representations of single AuNS (diameter of 40 nm) (A) and their random assemblies (dimer (B) and pentamer (C)) used in DDA calculations to simulate their optical absorption spectra shown in part D. It appears that the optical absorption band red-shifts as the nanospheres aggregates. (E) Plot showing the shift of the LSPR maxima as a function of the number of AuNSs. The spectra show that the number of the AuNS strongly affects the extent of the red-shift in the dipolar LSPR mode.

with high yield and monodispersity, which are critical for the optical performance of plasmonic nanostructures.[17]

Previously, we have demonstrated that nuclear targeting of nanoparticles can result in increased plasmonic field coupling and significant shift in their plasmon bands.[18,19] In view of developing novel therapeutic strategies, aggregation-induced plasmonic field shift in surface plasmon band of nanoparticles to the NIR region has enormous potential. Though aggregated nanoparticles showed promises in plasmonic photothermal therapy,[13,20−22] this approach has not been exploited to a greater extent. Moreover, some of these techniques require aggregating agents (e.g., salt) or aggregation-inducing functionalities on the nanoparticle surface.[20,23] Complicated synthetic and surface functionalization procedures associated with the preparation of individual or preaggregated nanoparticles as well as nonspecific heating of healthy cells due to the nonselective uptake of these nanoparticles remain as challenging issues, which might hamper their performance. Moreover, the photothermal conversion efficiency of such aggregated nanoparticles in PPT technique largely depends on several factors such as size, shape, and concentration of the nanoparticles, the number of nanoparticles internalized, types of cells, kinetics of aggregation of nanoparticles within the cells, etc.

Herein, we demonstrated both theoretically (using discrete dipolar approximation (DDA)) and experimentally that nuclear-targeted gold nanospheres (AuNSs), which poorly absorb light in the NIR region, become photothermally active by their spontaneous in situ assembly, selectively within the cancer cells. Though thermal conversion efficiency of aggregated AuNSs is not as good as NIR absorbing AuNRs,[24] localized plasmonic heating in the nuclear region of the cancer cells, which has been considered as the most thermolabile structures in the cells,[25] could provide selective and enhanced cancer cell ablation with minimal damage to the healthy cells. We systematically evaluated the efficacy of nuclear-targeted AuNSs in selective destruction of cancer cells with minimal damage to the healthy cells. Furthermore, plasmonic nanoparticles of various shapes such as cubes and rods have been exploited to unravel the role of plasmonic field coupling in assembled nanoparticles and their subsequent PPT killing efficiency at various stages of endocytosis. In order to validate the observed plasmonic photothermal phenomena, the NIR absorbing capabilities of aggregated AuNSs have been demonstrated both theoretically and experimentally.

RESULTS AND DISCUSSION

Among various applications of nanoparticles, plasmonic photothermal therapy, which utilizes the NIR absorbing capabilities of nanoparticles, has showed significant promise in cancer treatment. The interaction of light with plasmonic nanoparticles results in both the absorption and the scattering of light at the plasmon resonance frequency.[26] During the absorption processes, the nanoparticles utilize the energy of the incident light and convert it into heat.[27] It is well-known that NIR light penetrates human skin and reaches a number of in-body cancer locations.[1] The absorption of NIR light by the nanoparticles leads to enormous increase in its temperature around it, causing ablation or irreversible damage followed by cell death. Unlike NIR absorbing nanoparticles, AuNSs absorb light mostly in the visible region due to the resonance of coherent oscillations of the metal conducting electrons with visible light frequencies of light.[10] However, assembly of the AuNSs is likely to increase their NIR absorption efficiency in comparison to individual AuNS due to the formation of hot spots via enhanced plasmonic field coupling.[28,29] In order to find the effects of nanoparticle assemblies on the localized surface plasmon resonance (LSPR) band shift, random assemblies of 2 and 5 AuNSs (diameter of 40 nm) were generated and then their corresponding optical absorption

DOI: 10.1021/acs.bioconjchem.7b00427
Bioconjugate Chem. 2017, 28, 2452−2460

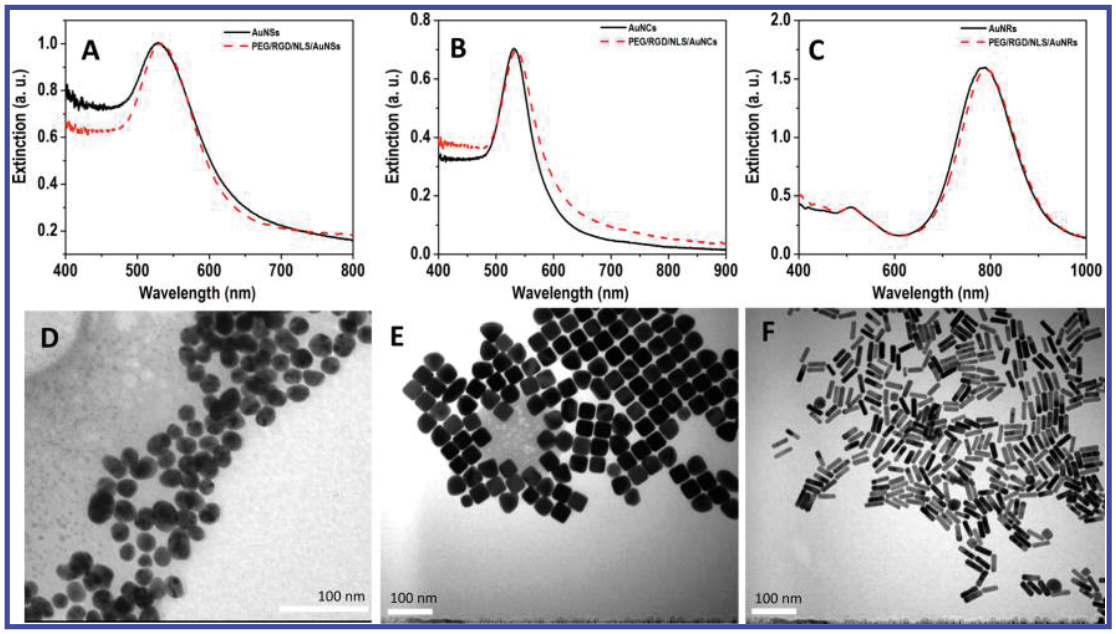

Figure 2. Parts A, B, and C are the extinction spectra of AuNSs, AuNCs, and AuNRs, respectively, collected before (black trace) and after (red trace) conjugation with PEG, RGD, and NLS. Parts D, E, and F are the TEM images of AuNSs, AuNCs, and AuNRs, respectively. A red-shift in the LSPR wavelength indicates the successful conjugation of the nanoparticles with PEG, RGD, and NLS.

spectra were simulated using discrete dipole approximation (DDA) (Figure 1).

It appears that when two AuNSs are assembled and positioned in close proximity (0.5 nm), their absorption wavelength significantly red-shifts as the dipolar plasmon oscillations couple via a short-range near-field coupling. Furthermore, the LSPR band was found to be red-shifted as the number of AuNSs increases. The theoretical results indeed showed that aggregation of the AuNSs clearly shifts the plasmonic band wavelength to longer wavelength by amounts that depend on the size of the aggregate so as to act as good photoabsorber in PPT. This encouraged us to use the in situ aggregation of the spherical nanoparticles within the cells, in the absence of any aggregation inducing agents, in the photothermal treatment of cancer cells.

In the present study, we exploited nuclear-targeted gold nanospheres (AuNSs) (diameter of ∼30 nm) and their in situ assembling capability around the nuclear region of the cells for the selective destruction of cancer cells with minimal damage to the healthy cells. We used nuclear-targeted AuNSs due to the fact that localized heating of the nuclear region of cells could potentially damage proteins of the nuclear matrix, which has been considered as one of the most thermolabile target sites within the cells as it can undergo denaturation at temperatures as low as 43−45 °C.[25] Perhaps this can induce cell death. Even though AuNSs show poor NIR absorption (as shown in our DDA simulations (Figure 1)), their in situ assembly during the endocytosis makes them good photoabsorbers in the NIR region of light and thereby a promising candidate in PPT. Other than AuNSs, plasmonic nanoparticles such as gold nanorods (AuNRs) (42 ± 4 nm in length and 13 ± 1.6 nm in width (∼3.2 aspect ratio)) and gold nanocubes (AuNCs) (edge length of ∼40 nm) were also used to study their efficiency as actively targeted plasmonic photothermal agents in selectively destroying cancer cells. The AuNSs, AuNCs, and AuNRs showed absorption maxima around 530, 535, and 790 nm, respectively. In order to reduce the cytotoxicity of the nanoparticles, the nanoparticles were functionalized with thiol containing methoxypolyethylene glycol (mPEG-SH) molecules. Besides that, the nanoparticles were further functionalized with RGD (peptide sequence capable of targeting $\alpha\beta$ integrins on the cancer cell membrane to facilitate the uptake of nanoparticles through receptor-mediated endocytosis)[30] and nuclear localization signaling (NLS) peptides. The NLS sequence helps the nanoparticles to target toward the nuclear region of the cells.[31] The ζ potential values collected before and after PEG, RGD, and NLS functionalization confirm the successful conjugation of the nanoparticles (Supporting Information Table S1).

Our previous studies showed that RGD and NLS functionalization of nanoparticles could help target the nuclear region of cells.[32,33] A red-shift of the LSPR band was observed after the functionalization of nanoparticles with PEG, RGD, and NLS. This indicates the successful conjugation of the nanoparticles with these molecules. The average size of the nanoparticles was further confirmed from the TEM images. The absorption spectra of each nanoparticle before and after conjugation with PEG, RGD, and NLS as well as their corresponding TEM images are given in Figure 2.

In this study, human oral squamous cell carcinoma 3 (HSC-3) and human keratinocyte (HaCaT) were used as cancerous and healthy cell models, respectively. All the experiments were performed with constant cell density as the endocytosis of nanoparticle largely depends on it. One of the main advantages of active targeting technique is that it can increase the overall intracellular concentration of nanoparticles at the target site (in this case, the nuclear region), which is inevitable in targeted nanomedicine. Also, precise targeting of cells with properly functionalized nanoparticles can minimize the off-site cellular toxicity. Figure 3 shows an illustration of various steps involved in targeting PEG/RGD/NLS/AuNSs to the nuclear region of the cells. This includes the binding of RGD peptide with $\alpha\beta$ integrins on the cell membrane to form a receptor−peptide complex, which facilitates the directional movement of AuNSs

DOI: 10.1021/acs.bioconjchem.7b00427
Bioconjugate Chem. 2017, 28, 2452−2460

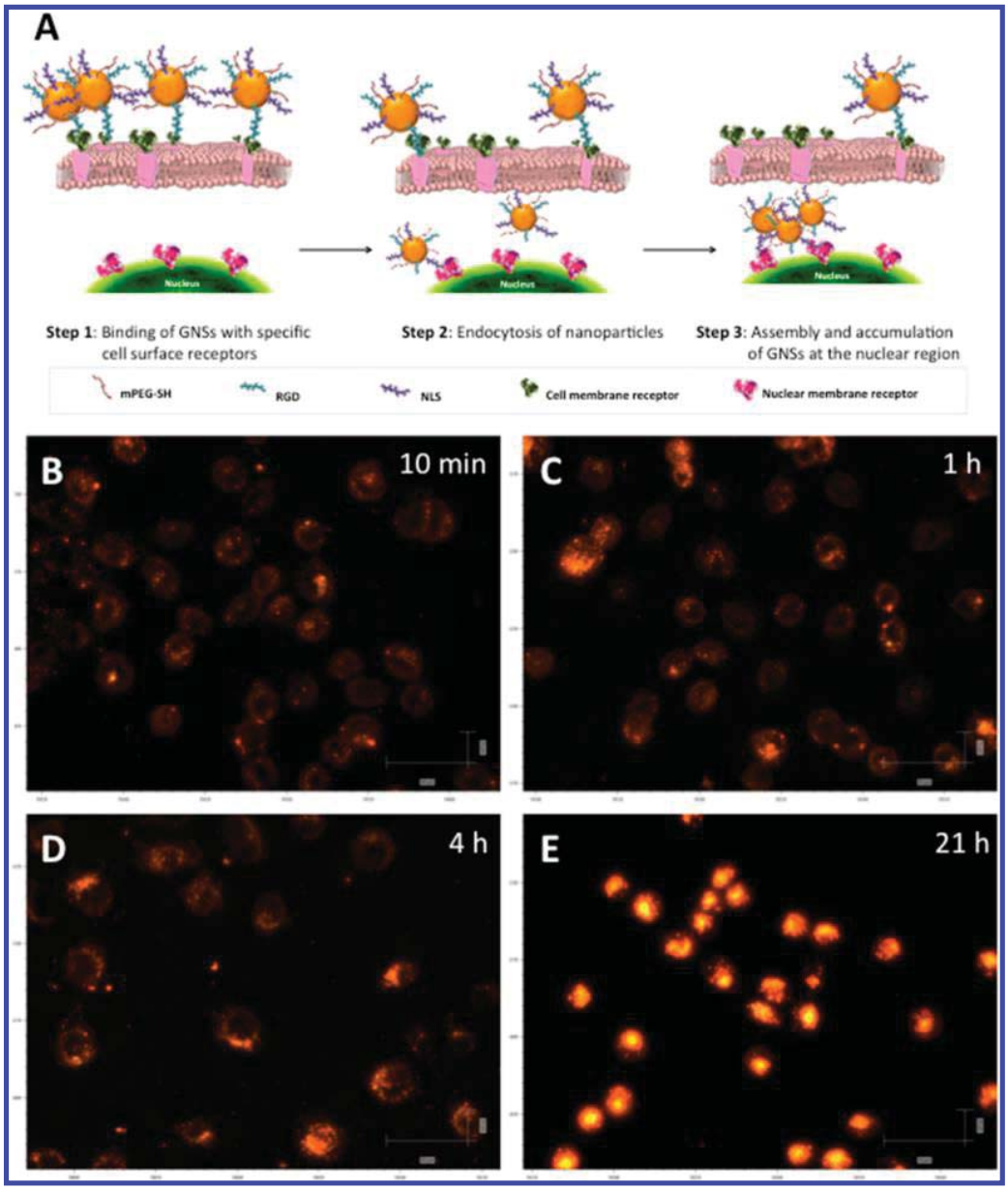

Figure 3. (A) Proposed mechanism of the interaction of PEG/RGD/NLS/AuNSs with the cancer cells and their subsequent endocytosis. Parts B−E are the dark-field microscopic images of HSC-3 cells collected at various stages of endocytosis of PEG/RGD/NLS/AuNSs ((B) 10 min, (C) 1 h, (D) 4 h, and (E) 21 h). After 21 h, it is obvious that nanoparticles are localized around the nuclear region of the HSC-3 cells.

toward clathrin-coated pits on the cell membrane.[34,35] While the RGD on the nanoparticle surface enhances their selective binding with $\alpha\beta$ integrin receptors and subsequent endocytosis of nanoparticles, nuclear targeting ligand, NLS, likely accelerates their accumulation at the nuclear region via selective interaction with nuclear import receptors.[32,36]

Augmented nuclear localization and assembly of the AuNSs are known to increase their scattering efficiency via enhanced plasmonic field coupling.[18] In order to determine the cellular uptake kinetics of the nanoparticles at various stages of the endocytosis, HSC-3 cells were incubated with nanoparticles at the same concentration (0.2 nM) for different periods of time (10 min, 1 h, 4 h, and 21 h). Dark-field (DF) microscopic images showing endocytosis of PEG/RGD/NLS/AuNSs to HSC-3 cells collected at various time intervals are given in Figure 3. It is obvious from the DF images that the intensity of scattering of the particle within the cells gradually enhances as the endocytosis progresses, which implies the internalization of the nanoparticles into the cytoplasm of the cells and their subsequent assembly at the nuclear region of the cells. Even though the exact mechanism of formation of nanoparticles aggregates inside the live cells is unclear, during the endocytosis, the nanoparticles are expected to be exposed to highly dynamic intracellular biological environment, which can induce nanoparticle aggregation via surface destabilization induced by various factors such as change in ionic strength, nanoparticles−protein interactions, pH, etc. We monitored the cellular uptake only for 21 h as the cell cycle of HSC-3 cells complete in ∼24 h[37] and further treatment will reduce the intracellular nanoparticle density as a result of cell division and distribute their intracellular nanoparticles to the daughter cells. The rate of endocytosis of nanoparticles to the cancer cells was

DOI: 10.1021/acs.bioconjchem.7b00427
Bioconjugate Chem. 2017, 28, 2452−2460

studied by using both absorption spectroscopy and dark-field imaging microscopy. In this study, the cells were grown on a coverslip for 24 h, which were then incubated with nanoparticles (PEG/RGD/NLS/AuNSs and PEG/RGD/NLS/AuNRs) for various periods of time. This culture medium containing nanoparticles was aspirated at regular intervals of time, and the extinction spectra were noted.

Figure 4 shows the percentage of uptake of PEG/RGD/NLS/AuNSs as well as PEG/RGD/NLS/AuNRs by HSC-3

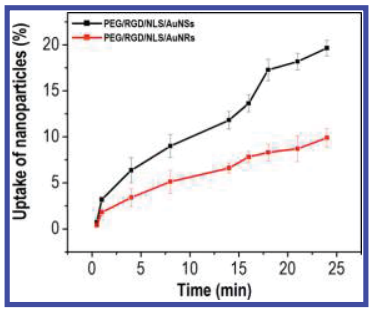

Figure 4. Plots showing percentage of uptake of PEG/RGD/NLS/AuNSs and PEG/RGD/NLS/AuNRs by HSC-3 cells as a function of time. In comparison to AuNSs, AuNRs showed a ~2-fold decrease in the cellular uptake by HSC-3 cells.

cells plotted against their incubation time. We notice that significant amount of nanoparticles remained in the solution even after 24 h of incubation with the HSC-3 cells with the nanoparticles. Between the two nanoparticles, AuNRs showed ~2-fold decrease in the uptake than AuNSs. The dark-field images collected from the HSC-3 cells, which are treated with PEG/RGD/NLS/AuNRs for 21 h, further validated this observation (see Supporting Information Figure S1). A decrease in the scattering intensity of the cells in comparison to AuNSs was obvious in the dark-field images.

In order to study the plasmonic heat generation and photothermal conversion efficiency of AuNSs and their aggregates, we prepared aggregates of AuNSs having extinction maxima at ~735 nm and ~767 nm (Figure 5). In this study, bare Au@citrate nanospheres, prior to the PEG/RGD/NLS functionalization, were used. Here, phosphate buffered saline (PBS) was used as an aggregation-inducing agent as a relatively high ionic strength of PBS could lead to the destabilization of the Au@citrate nanospheres and subsequent aggregation. These samples were irradiated with 808 nm CW laser with a power density of ~5W/cm^2 for 2 min, and the temperature was monitored at 1 min intervals. The initial temperature of the solution was kept at around 35 ± 2 °C, and an increase in temperature was monitored at regular intervals and was plotted against time (Figure 5D). Even though the aggregation of the nanoparticles significantly reduced the intensity of extinction in comparison to the parent AuNSs solution, the solution of AuNSs aggregate with extinction maximum at ~767 showed temperature increase up to 62.2 ± 2 °C after 2 min of laser irradiation.

Intracellular aggregation of nanoparticles was further confirmed by the TEM images of the cells, which were incubated with PEG/RGD/NLS/AuNSs for 1 and 21 h (Figure 6). Here, the cells were incubated with the nanoparticles in a Petri dish and the nanoparticle solution was aspirated after 1 or 21 h. Afterward, the cells were trypsinized and were washed once with DI water. For partial cell rupturing, the cells were

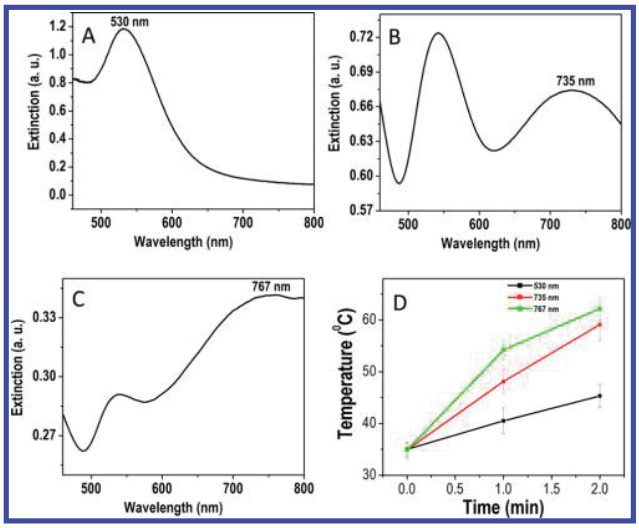

Figure 5. Parts A–C are the extinction spectra of parent AuNSs and their aggregates showing different extinction maxima. (D) Plots showing an increase in temperature induced by PPT heating of AuNSs and the aggregates upon exposure to 808 nm laser excitation for 1 and 2 min. AuNSs aggregates with extinction maximum at ~767 nm showed the largest temperature increase of ~62.2 °C after 2 min of laser irradiation. Exposure of the parent AuNSs with the laser for 2 min only resulted in a maximum temperature of ~45.3 °C after 2 min. The temperature of all solutions prior to the laser exposure was kept at 36 ± 1 °C.

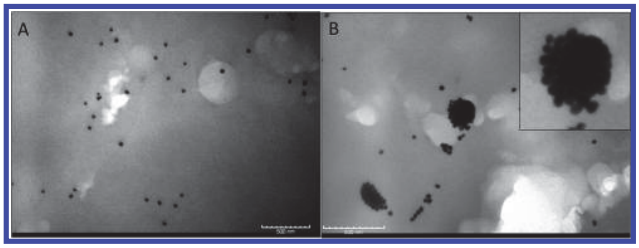

Figure 6. TEM images collected from the HSC-3cells incubated with PEG/RGD/NLS AuNSs for 1 h (A) and 21 h (B). The inset of panel B is an enlarged view of the aggregated nanoparticles. The samples were prepared by partially rupturing the cells by gentle sonication.

gently sonicated for 10 s and drop-casted on a carbon-coated copper grid for TEM analysis. We did gentle sonication in order to preserve the morphology of the aggregate within the cells with minimal deformation. The TEM image collected from the cell sample, which was incubated with the nanoparticles for 1 h, showed random distribution of individual spherical nanoparticles throughout the TEM grid (Figure 6A).

The cells incubated with nanoparticles for 21 h showed the presence of aggregated nanoparticles of an overall size larger than 200 nm (Figure 6B). Aggregates containing various numbers of nanoparticles ranging from 10 to 100 nanoparticles were also visible on the TEM grid.

We systematically demonstrated that endocytosis of targeted nanoparticles can result in their accumulation and formation of stable aggregates specifically within the HSC-3 cancer cells. Moreover, the PEG, RGD, and NLS-conjugated AuNSs, AuNCs, and AuNRs used in our studies showed excellent biocompatibility (Supporting Information Figure S2). The intracellular aggregates formed inside the cells are capable of absorbing light in the NIR region of light as their extinction

DOI: 10.1021/acs.bioconjchem.7b00427
Bioconjugate Chem. 2017, 28, 2452–2460

maxima significantly overlap with the wavelength of the excitation laser. As a result, a systematic variation in the percentage of cell death was observed when the cells were exposed to the laser at various stages of the endocytosis (Figure 7), which was probed by standard XTT assay. HSC-3 cells

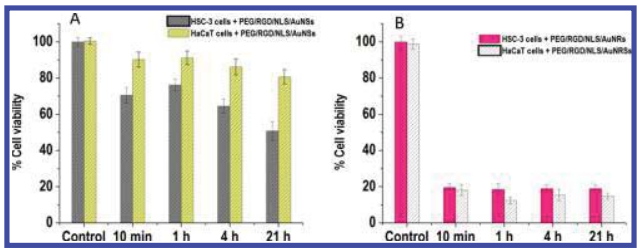

Figure 7. Cell viability for HSC-3 and HaCaT cells treated with 0.2 nM PEG/RGD/NLS conjugated AuNSs (A) and AuNRs (B) solutions followed by laser exposure for 5 min to induce cell death.

exposed to the 808 nm laser exhibited nearly 99% cell viability, which confirms that the cell death due to the absorption of the incident laser by the cell itself is negligible. At the same time, a marginal cell death was expected just after the treatment of cells with targeted AuNSs following laser exposure. This is due to the fact that the absorption of 808 nm laser light by the AuNSs is expected to be very low due to the poor overlap of their surface plasmon resonance band (530 nm) with the excitation laser wavelength. However, ~30% of cell death was observed when the HSC-3 cells were treated with PEG/RGD/NLS/AuNSs for 10 min followed by laser irradiation for 5 min.

One possible explanation for this observation could be the enhanced docking of the nanoparticles on the cell membrane as a result of the binding of RGD peptide present on the PEG/RGD/NLS/AuNSs surface with the receptor integrin proteins on the cancer cell surface. This may result in the formation of a temporary assembly of the nanoparticle on the cell surface as shown in Figure 3A. The plasmonic coupling in such assemblies could absorb the light in the NIR region (this has been validated numerically) and induce photothermal cell ablation. As the endocytosis progressed, a decrease in the cell death (~25%) was observed after 1 h. This observed behavior could result from the internalization of the receptor bound nanoparticles from the cell membrane to the cytoplasm and subsequent weakening of the plasmonic field coupling phenomena of the nanoparticles. Note that the process of internalization of the nanoparticle is fast and can happen even after 20 min of incubation.[38] After 4 h of incubation, the cell viability further decreased to ~65%, which could be attributed to the assembly of the nanoparticles in the nuclear region of the cell, whereas a significant decrease (~50%) in the cell viability was observed for cells incubated with PEG/RGD/NLS/AuNSs for 21 h followed by laser irradiation for 5 min. These results indicate that longer incubation time of cells with nuclear-targeted nanoparticles can promote their aggregation near the nuclear region followed by significant absorption in the NIR region of light and subsequent cell death by possible damage to the proteins of the nuclear matrix. In addition, we confirmed that no PPT cell death happens when PEG/AuNSs were used instead (Supporting Information Figure S3). Here, the absence of RGD and NLS significantly reduces the cellular internalization of PEG/AuNSs and their localization near the nuclear region. This result further validates the significant role of localized plasmonic heating around the nuclear region in killing the cancer cells.

In order to study the selectivity of our technique in cancer cell targeting and to confirm that indeed aggregation of nanoparticle is taking place largely in the nuclear region of the cancer cells, we conducted control experiments on healthy HaCaT cells as they do not overexpress $\alpha\beta$-integrins[39] and thereby exhibit relatively lower uptake of PEG/RGD/NLS/AuNSs. In comparison to the HSC-3 cells, HaCaT cells exhibited relatively lower cellular uptake of PEG/RGD/NLS/AuNSs, which was confirmed from the dark-field images collected at various periods of time (Supporting Information Figure S4). Even after incubation of the HaCaT cells with these nanoparticles for 21 h, only ~20% cell death was observed, which clearly indicates the selectivity of this technique toward killing cancer cells with minimal damage to healthy cells. Furthermore, we demonstrated the selectivity of this technique to minimize off-site cellular toxicity in comparison to AuNRs (Figure 7). Here, irradiation of both HSC-3 and HaCaT cells treated with 0.2 nM PEG/RGD/NLS/AuNRs for different periods of time (10 min, 1 h, 4 h, and 21 h) with 808 nm laser for 5 min resulted in significant amount of cell death in all the cases (>80%). This could be attributed to the fact that the PEG/RGD/NLS/AuNR used in these studies exhibited longitudinal surface plasmon resonance band at ~790 nm, which could absorb the 808 nm laser to a greater extent and induce photothermal ablation of the cells regardless of the types of cells and percentage of uptake of nanoparticles. The AuNRs in the media and internalized by the cells are capable of absorbing a large portion of the 808 nm laser and could induce cell ablation. In contrast, relatively lower cell death (<20%) was observed for the HaCaT cells treated with PEG/RGD/NLS/AuNSs for 21 h followed by laser exposure for 5 min due to their poor nanoparticle uptake, which clearly implies the selectivity of this technique in targeting cancer cells.

To further validate PPT efficacy, we also carried out trypan blue assay that utilizes membrane integrity to identify dead cells. Here, the dead cells will be selectively stained by trypan blue, as the cell membrane is permeable to the trypan blue dye. However, the live cells will remain unstained. Extensive cell death (>90%) was obvious in AuNRs-treated HSC-3 and HaCaT cells (Figure 8C and Figure 8D) for 4 h followed by laser exposure for 5 min, whereas ~85% of AuNSs-treated HaCaT cells remained viable after laser treatment (Figure 8A). Interestingly, ~40% cell death was observed for HSC-3 cells (treated with AuNSs for 4 h) exposed to the laser for 5 min (Figure 8B). These results show that selective killing of cancer cells can be achieved by brief laser exposure of PEG/RGD/NLS/AuNSs-treated cancer cells.

To further demonstrate the potential of this technique in selectively killing the cancer cells, we conducted similar experiments with PEG/RGD/NLS/AuNCs, which show surface plasmon resonance band at ~538 nm. As in the case of PEG/RGD/NLS/AuNSs, AuNCs showed a similar trend in selective cancer cell ablation (see Supporting Information Figure S5), though the efficiency was relatively lower compared to PEG/RGD/NLS/AuNSs. This could possibly be due to the poor overlap of intracellular aggregates with the excitation laser wavelength.

■ CONCLUSION

We demonstrated a cancer cell specific plasmonic photothermal therapeutic (PPT) paradigm that utilizes the inherent in situ

DOI: 10.1021/acs.bioconjchem.7b00427
Bioconjugate Chem. 2017, 28, 2452−2460

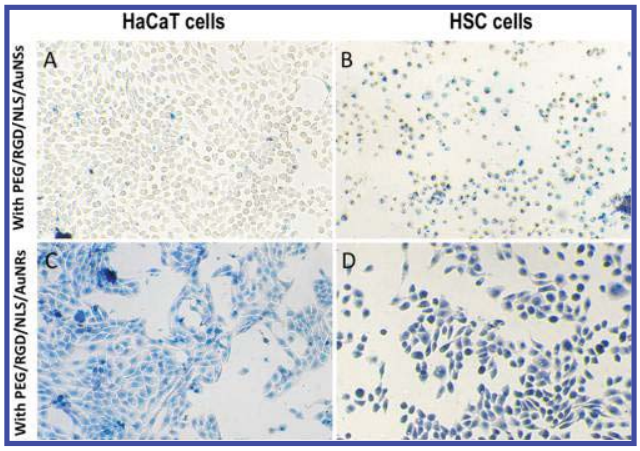

Figure 8. HaCaT (A, C) and HSC-3 (B, D) cells incubated with PEG/RGD/NLS/AuNSs (A, B) and PEG/RGD/NLS/AuNRs (C, D) for 4 h followed by exposure to 808 nm laser for 5 min and then stained with trypan blue. Here, dead cells are selectively stained by trypan blue (as the cell membrane is permeable to the trypan blue dye), while live cells remain unstained.

self-assembling property and subsequent enhanced NIR absorbing capability of nuclear-targeted AuNSs specifically within the cancer cells to selectively destroy cancer cells with minimal damage to healthy cells. Furthermore, plasmonic nanoparticles of other shapes such as cubes and rods have been exploited to systematically elucidate the role of plasmonic field coupling in assembled nanoparticles and subsequent PPT killing efficiency at various stages of endocytosis. In comparison to the previous reports on utilizing aggregated plasmonic nanoparticles in PPT-based cancer treatment, our technique utilized the localized plasmonic heating phenomena at the nuclear region of the cells where the nuclear matrix proteins are largely found, which has been considered as one of the most thermolabile structures within the cells, to deliver selective and enhanced cell ablation of cancer cells with minimal damage to the healthy cells. The plasmonic field coupling and related plasmonic photothermal heating properties of assembled nanoparticles were further demonstrated both experimentally and theoretically using DDA approximation. Taking advantage of intracellular assembling phenomena of nuclear-targeted nanoparticles could be extended to various other nanoparticles, which could exhibit enhanced NIR absorbing capability upon aggregation and could potentially lead to the development of more efficient and selective PPT-based cancer treatment modalities with minimal side effect.

MATERIALS AND METHODS

(a) Materials. Hydrogen tetrachloroaurate trihydrate aqueous solution ($HAuCl_4 \cdot 3H_2O$), sodium borohydride ($NaBH_4$), ascorbic acid, $AgNO_3$, cetyltrimethylammonium bromide (CTAB), trypan blue, and trisodium citrate were purchased from Sigma-Aldrich, USA. Custom-made RGD (RGDRGDRGDRGDPGC) and NLS (CGGGPKKKRKVGG) peptides were purchased from GenScript USA, Inc. Thiol-modified methoxypolyethylene glycol (mPEG-SH) of MW 5000 was obtained from Laysan Bio, Inc.

(b) Instrumentation. Dark-field images of cells under various experimental conditions were collected using Leica microscope coupled with a Renishaw inVia Raman microscope. A JEOL 100CX-2 microscope was used to collect the transmission electron microscopic (TEM) images. The average diameters of AuNSs, AuNRs, and AuNCs were determined using ImageJ software. UV−vis extinction spectra were collected using an Ocean Optics HR4000CG-UV-NIR spectrometer. ζ potentials of the nanoparticles were measured using a Malvern Zetasizer Nano Z.

(c) Synthesis of Gold Nanospheres (~30 nm Diameter). Gold nanospheres (AuNSs) were prepared by following modified Turkevich approach.[40] Briefly, 140 mL of 1% $HAuCl_4 \cdot 3H_2O$ solution in DI water was brought to boiling, and 0.2% trisodium citrate trihydrate (2.5 mL) was added. The solution was heated and stirred until the solution turned to red wine color. The resultant AuNSs solution was allowed to cool down to the room temperature.

(d) Synthesis of Gold Nanocubes (~40 nm Edge Length). Gold nanocubes (AuNCs) were prepared as per the procedure described in our previous papers.[41,42] The seed nanoparticles were prepared by the reduction of 275 μL of $HAuCl_4 \cdot 3H_2O$ (10 mM), which is added to a solution of 7 mL of 100 mM CTAB prepared in deionized water (DI), by 600 μL of an ice cold 0.01 M $NaBH_4$ solution under stirring for 2 min. After 1 h, 350 μL of 10-fold diluted seed solution was allowed to grow for 4 h in a growth solution. The growth solution was prepared by mixing CTAB solution (2.916 g dissolved in 400 mL of DI water) with $HAuCl_4 \cdot 3H_2O$ solution (0.0394 g dissolved in 143 mL of DI water) followed by adding 6 mL (1 M) of ascorbic acid. The resultant CTAB stabilized AuNCs were purified by centrifugation and redispersion in DI water.

(e) Synthesis of Au NRs. Gold nanorods were synthesized by the modified seed-mediated protocol.[43] Briefly, the seed nanoparticles were synthesized by adding 250 μL of $HAuCl_4$ (10 mM) to 7 mL of CTAB (0.1 M) followed by the addition of 600 μL of an ice-cold 10 mM $NaBH_4$ solution under stirring for 2 min. After 1 h, 400 μL of seed solution was added to the growth solution, which was prepared by mixing of 40 mL of CTAB (100 mM) with 1.7 mL of $HAuCl_4$ (10 mM), 250 μL of $AgNO_3$ (10 mM), and 270 μL of ascorbic acid (100 mM). After the addition of seed solution, the entire solution was kept undisturbed for 6 h. The as prepared AuNRs solution was purified by centrifugation.

(f) Preparation of PEG/RGD/NLS-Functionalized Gold Nanoparticles. In order to reduce the cytotoxicity of the gold nanoparticles (AuNSs, AuNCs, or AuNRs), they were first functionalized with mPEG-SH. Here, 15 mL of 0.2 nM AuNCs solution was incubated with 90 μL of mPEG-SH (1 mM) for 24 h. Similarly, to conjugate AuNSs with mPEG-SH, 5 mL of 3 nM AuNSs solution was treated with 30 μL of 1 mM mPEG-SH solution for 24 h. PEGylated AuNRs were prepared by treating 10 mL of 5 nM AuNRs with 50 μL of mPEG-SH solution (1 mM). Afterward, the PEGylated nanoparticles were treated with RGD and NLS with a ratio of 4:10 to yield PEG/RGD/NLS-functionalized nanoparticles. The nanoparticles at different stages of preparation were purified by centrifugation to remove unbound ligands.

(g) Cellular Uptake Studies. The percentage of cellular uptake of the nanoparticles by HSC-3 cells was determined by culturing the cells in 12-well tissue culture plate overnight and subsequent replacement of media with 0.2 nM PEG/RGD/NLS conjugated nanoparticles (AuNSs or AuNRs) prepared in culture media (without phenol red). The cells were incubated with the nanoparticles for different time intervals. Afterward, the optical density of the media was measured at regular intervals to find out the percentage of uptake of the

DOI: 10.1021/acs.bioconjchem.7b00427
Bioconjugate Chem. 2017, 28, 2452−2460

nanoparticles. To calculate the percentage of cellular uptake, the optical density of AuNPs containing culture media collected at regular intervals was subtracted from the optical density of nanoparticles initially added to the cell culture.

(h) Photothermal Heating of AuNSs Solutions. A 100 μL solution of AuNSs and aggregated AuNSs solutions (showing different absorption maxima) were added to 96-well plates to mimic the cellular PPT experiments. The solutions were then exposed to the 808 nm CW laser. The temperatures of the solution at 1 and 2 min were measured by directly placing a thermocouple into the solutions. Three independent experiments were conducted and the mean ± sd of the thermal responses was plotted as a function of laser irradiation time.

(i) Plasmonic Photothermal Heating of Cells. For the PPT studies, the cells (HSC-3 and HaCaT) were grown for 48 h in 96-well tissue culture plates. Upon reaching 70% confluence, the growth medium was replaced with medium containing PEG-conjugated NPs (AuNSs, AuNCs, or AuNRs) at a concentration of 0.2 nM. After incubation of the cells for various time intervals, the cells were exposed to the 808 nm laser. The cells were incubated for another 30 min, and then the medium was replaced with culture medium (without phenol red) containing the XTT cell viability assay solution. The cell viability of the PPT treated HSC-3 and HaCaT cells was then determined according to the manufacturer's protocol.

For trypan blue assay, after the laser irradiation, 100 μL of 1:1 solution of 0.4% trypan blue (Sigma) in PBS solution was added to the wells and they were left for 10 min for staining. After staining, the cells are rinsed with PBS buffer and kept in the buffer for bright field imaging.

(j) Cell Culture. The cells were cultured in Dulbecco's modified Eagle's medium (DMEM, Mediatech), with phenol red, supplemented with 10% v/v fetal bovine serum (FBS, Mediatech) and 1% antimycotic solution (Mediatech) in a 37 °C, 5% CO_2 humidified incubator. For the dark-field imaging studies, the cells were grown on glass coverslips in complete growth medium at 37 °C for 24 h. Afterward, the cells were incubated with 0.2 nM PEG/RGD/NLS-functionalized nanoparticles (AuNSs, AuNCs, or AuNRs) diluted in supplemented DMEM cell culture medium, and the dark-field images were collected at regular time intervals.

(k) Is the Plasmonic Wavelength of the Assembled Spherical Gold Nanoparticles Sensitive to Its Degree of Aggregation? Theoretical Investigation. For these calculations, the discrete-dipole approximation (DDA),[44] one of the most powerful theoretical techniques to model the optical properties of plasmonic nanoparticles of arbitrary geometries, has been used to simulate the effects of nanoparticle assemblies on the LSPR band shift. The DDA method numerically solves Maxwell's equations for one or more arbitrary shapes by dividing each shape into a cubic array of polarizable dipole points. The corresponding response of N dipole points to the incident electromagnetic field and all other $N - 1$ dipole points are solved self-consistently using Maxwell's equations. Here, the assemblies of AuNSs for DDA simulation were generated via free tools available on https://nanoHUB.org. The DDA method was used to calculate near-field interaction between the AuNSs (40 nm in diameter). The surrounding medium was assumed to be water (n = 1.33), and the refractive index of AuNSs was assumed to be the same as that of the bulk metal.[45] For each case (single, dimer, and pentamer) the interparticle distance was fixed as 0.5 nm. The incident light was polarized along the interparticle axis of the AuNSs systems. The theoretical and experimental results indeed suggested that aggregations of AuNSs could possibly make them absorb light in the NIR region, depending on the size of aggregate.

■ ASSOCIATED CONTENT

Supporting Information

The Supporting Information is available free of charge on the ACS Publications website at DOI: 10.1021/acs.bioconjchem.7b00427.

Additional dark-field images showing the cellular uptake of AuNRs, ζ potential values, supporting cell viability data (PDF)

■ AUTHOR INFORMATION

Corresponding Author

*E-mail: melsayed@gatech.edu. Phone: 404-894-0292. Fax: 404-894-0294.

ORCID

Sajanlal R. Panikkanvalappil: 0000-0002-8337-9591

Mostafa A. El-Sayed: 0000-0002-7674-8424

Notes

The authors declare no competing financial interest.

■ ACKNOWLEDGMENTS

This work was supported by NSF-DMR (Grant 1644354). Mena Aioub is thanked for help with the TEM measurements.

■ REFERENCES

(1) Huang, X., El-Sayed, I. H., Qian, W., and El-Sayed, M. A. (2006) Cancer cell imaging and photothermal therapy in the near-infrared region by using gold nanorods. *J. Am. Chem. Soc. 128*, 2115−2120.

(2) Lal, S., Clare, S. E., and Halas, N. J. (2008) Nanoshell-enabled photothermal cancer therapy: Impending clinical impact. *Acc. Chem. Res. 41*, 1842−1851.

(3) Aioub, M., Panikkanvalappil, S. R., and El-Sayed, M. A. (2017) Platinum-coated gold nanorods: Efficient reactive oxygen scavengers that prevent oxidative damage toward healthy, untreated cells during plasmonic photothermal therapy. *ACS Nano 11*, 579−586.

(4) Zou, L., Wang, H., He, B., Zeng, L., Tan, T., Cao, H., He, X., Zhang, Z., Guo, S., and Li, Y. (2016) Current approaches of photothermal therapy in treating cancer metastasis with nanotherapeutics. *Theranostics 6*, 762−772.

(5) Dreaden, E. C., Mackey, M. A., Huang, X., Kang, B., and El-Sayed, M. A. (2011) Beating cancer in multiple ways using nanogold. *Chem. Soc. Rev. 40*, 3391−3404.

(6) Jain, P. K., Huang, X., El-Sayed, I. H., and El-Sayed, M. A. (2008) Noble metals on the nanoscale: Optical and photothermal properties and some applications in imaging, sensing, biology, and medicine. *Acc. Chem. Res. 41*, 1578−1586.

(7) Abadeer, N. S., and Murphy, C. J. (2016) Recent progress in cancer thermal therapy using gold nanoparticles. *J. Phys. Chem. C 120*, 4691−4716.

(8) Shanmugam, V., Selvakumar, S., and Yeh, C. S. (2014) Near-infrared light-responsive nanomaterials in cancer therapeutics. *Chem. Soc. Rev. 43*, 6254−6287.

(9) Zhang, Z., Wang, J., and Chen, C. (2013) Near-infrared light-mediated nanoplatforms for cancer thermo-chemotherapy and optical imaging. *Adv. Mater. 25*, 3869−3880.

(10) Huang, X., and El-Sayed, M. A. (2010) Gold nanoparticles: Optical properties and implementations in cancer diagnosis and photothermal therapy. *J. Adv. Res. 1*, 13−28.

(11) Perez-Hernandez, M., Del Pino, P., Mitchell, S. G., Moros, M., Stepien, G., Pelaz, B., Parak, W. J., Galvez, E. M., Pardo, J., and de la Fuente, J. M. (2015) Dissecting the molecular mechanism of apoptosis

DOI: 10.1021/acs.bioconjchem.7b00427
Bioconjugate Chem. 2017, 28, 2452−2460

during photothermal therapy using gold nanoprisms. *ACS Nano 9*, 52−61.
(12) Chen, J., Wang, D., Xi, J., Au, L., Siekkinen, A., Warsen, A., Li, Z. Y., Zhang, H., Xia, Y., and Li, X. (2007) Immuno gold nanocages with tailored optical properties for targeted photothermal destruction of cancer cells. *Nano Lett. 7*, 1318−1322.
(13) Espinosa, A., Silva, A. K., Sanchez-Iglesias, A., Grzelczak, M., Pechoux, C., Desboeufs, K., Liz-Marzan, L. M., and Wilhelm, C. (2016) Cancer cell internalization of gold nanostars impacts their photothermal efficiency in vitro and in vivo: Toward a plasmonic thermal fingerprint in tumoral environment. *Adv. Healthcare Mater. 5*, 1040−1048.
(14) Sykes, E. A., Chen, J., Zheng, G., and Chan, W. C. (2014) Investigating the impact of nanoparticle size on active and passive tumor targeting efficiency. *ACS Nano 8*, 5696−5706.
(15) Matsumura, Y., and Maeda, H. (1986) A new concept for macromolecular therapeutics in cancer chemotherapy: Mechanism of tumoritropic accumulation of proteins and the antitumor agent smancs. *Cancer. Res. 46*, 6387−6392.
(16) Schroeder, A., Heller, D. A., Winslow, M. M., Dahlman, J. E., Pratt, G. W., Langer, R., Jacks, T., and Anderson, D. G. (2011) Treating metastatic cancer with nanotechnology. *Nat. Rev. Cancer 12*, 39−50.
(17) Qin, Z., Wang, Y., Randrianalisoa, J., Raeesi, V., Chan, W. C., Lipinski, W., and Bischof, J. C. (2016) Quantitative comparison of photothermal heat generation between gold nanospheres and nanorods. *Sci. Rep. 6*, 29836.
(18) Aioub, M., Kang, B., Mackey, M. A., and El-Sayed, M. A. (2014) Biological targeting of plasmonic nanoparticles improves cellular imaging via the enhanced scattering in the aggregates formed. *J. Phys. Chem. Lett. 5*, 2555−2561.
(19) Qian, W., Huang, X., Kang, B., and El-Sayed, M. A. (2010) Dark-field light scattering imaging of living cancer cell component from birth through division using bioconjugated gold nanoprobes. *J. Biomed. Opt. 15*, 046025.
(20) Sun, M., Liu, F., Zhu, Y., Wang, W., Hu, J., Liu, J., Dai, Z., Wang, K., Wei, Y., Bai, J., et al. (2016) Salt-induced aggregation of gold nanoparticles for photoacoustic imaging and photothermal therapy of cancer. *Nanoscale 8*, 4452−4457.
(21) Nam, J., Won, N., Jin, H., Chung, H., and Kim, S. (2009) pH-induced aggregation of gold nanoparticles for photothermal cancer therapy. *J. Am. Chem. Soc. 131*, 13639−13645.
(22) Yang, Y., Hu, Y., Du, H., and Wang, H. (2014) Intracellular gold nanoparticle aggregation and their potential applications in photodynamic therapy. *Chem. Commun. 50*, 7287−7290.
(23) Li, H., Liu, X., Huang, N., Ren, K., Jin, Q., and Ji, J. (2014) "Mixed-charge self-assembled monolayers" as a facile method to design ph-induced aggregation of large gold nanoparticles for near-infrared photothermal cancer therapy. *ACS Appl. Mater. Interfaces 6*, 18930−18937.
(24) Chen, H., Shao, L., Ming, T., Sun, Z., Zhao, C., Yang, B., and Wang, J. (2010) Understanding the photothermal conversion efficiency of gold nanocrystals. *Small 6*, 2272−2280.
(25) Roti Roti, J. L., Kampinga, H. H., Malyapa, R. S., Wright, W. D., vanderWaal, R. P., and Xu, M. (1998) Nuclear matrix as a target for hyperthermic killing of cancer cells. *Cell Stress Chaperones 3*, 245−255.
(26) Bohren, C. F., and Huffman, D. R. (2007) Extinction. In *Absorption and Scattering of Light by Small Particles* pp 286−324, Wiley-VCH Verlag GmbH.
(27) Link, S., and El-Sayed, M. A. (2000) Shape and size dependence of radiative, non-radiative and photothermal properties of gold nanocrystals. *Int. Rev. Phys. Chem. 19*, 409−453.
(28) Norman, T. J., Grant, C. D., Magana, D., Zhang, J. Z., Liu, J., Cao, D., Bridges, F., and Van Buuren, A. (2002) Near infrared optical absorption of gold nanoparticle aggregates. *J. Phys. Chem. B 106*, 7005−7012.
(29) Jain, P. K., Lee, K. S., El-Sayed, I. H., and El-Sayed, M. A. (2006) Calculated absorption and scattering properties of gold nanoparticles of different size, shape, and composition: Applications in biological imaging and biomedicine. *J. Phys. Chem. B 110*, 7238−7248.
(30) Garrigues, H. J., Rubinchikova, Y. E., Dipersio, C. M., and Rose, T. M. (2008) Integrin alpha$_v$beta$_3$ binds to the rgd motif of glycoprotein b of kaposi's sarcoma-associated herpesvirus and functions as an rgd-dependent entry receptor. *J. Virol. 82*, 1570−1580.
(31) Freitas, N., and Cunha, C. (2009) Mechanisms and signals for the nuclear import of proteins. *Curr. Genomics 10*, 550−557.
(32) Kang, B., Mackey, M. A., and El-Sayed, M. A. (2010) Nuclear targeting of gold nanoparticles in cancer cells induces DNA damage, causing cytokinesis arrest and apoptosis. *J. Am. Chem. Soc. 132*, 1517−1519.
(33) Panikkanvalappil, S. R., Hira, S. M., Mahmoud, M. A., and El-Sayed, M. A. (2014) Unraveling the biomolecular snapshots of mitosis in healthy and cancer cells using plasmonically-enhanced Raman spectroscopy. *J. Am. Chem. Soc. 136*, 15961−15968.
(34) Sorkin, A., and Puthenveedu, M. A. (2013) Clathrin-mediated endocytosis. In *Vesicle Trafficking in Cancer* (Yarden, Y., and Tarcic, G., Eds.) pp 1−31, Springer New York, New York, NY.
(35) Zhang, S., Gao, H., and Bao, G. (2015) Physical principles of nanoparticle cellular endocytosis. *ACS Nano 9*, 8655−8671.
(36) Tkachenko, A. G., Xie, H., Coleman, D., Glomm, W., Ryan, J., Anderson, M. F., Franzen, S., and Feldheim, D. L. (2003) Multifunctional gold nanoparticle-peptide complexes for nuclear targeting. *J. Am. Chem. Soc. 125*, 4700−4701.
(37) Kang, B., Austin, L. A., and El-Sayed, M. A. (2012) Real-time molecular imaging throughout the entire cell cycle by targeted plasmonic-enhanced Rayleigh/Raman spectroscopy. *Nano Lett. 12*, 5369−5375.
(38) Zhang, S., Li, J., Lykotrafitis, G., Bao, G., and Suresh, S. (2009) Size-dependent endocytosis of nanoparticles. *Adv. Mater. 21*, 419−424.
(39) Koivisto, L., Larjava, K., Hakkinen, L., Uitto, V. J., Heino, J., and Larjava, H. (1999) Different integrins mediate cell spreading, haptotaxis and lateral migration of hacat keratinocytes on fibronectin. *Cell. Adhes. Commun. 7*, 245−257.
(40) Turkevich, J., Stevenson, P. C., and Hillier, J. (1951) A study of the nucleation and growth processes in the synthesis of colloidal gold. *Discuss. Faraday Soc. 11*, 55−75.
(41) Panikkanvalappil, S. R., James, M., Hira, S. M., Mobley, J., Jilling, T., Ambalavanan, N., and El-Sayed, M. A. (2016) Hyperoxia induces intracellular acidification in neonatal mouse lung fibroblasts: Real-time investigation using plasmonically enhanced Raman spectroscopy. *J. Am. Chem. Soc. 138*, 3779−3788.
(42) Panikkanvalappil, S. R., Hira, S. M., and El-Sayed, M. A. (2016) Elucidation of ultraviolet radiation-induced cell responses and intracellular biomolecular dynamics in mammalian cells using surface-enhanced Raman spectroscopy. *Chem. Sci. 7*, 1133−1141.
(43) Nikoobakht, B., and El-Sayed, M. A. (2003) Preparation and growth mechanism of gold nanorods (NRs) using seed-mediated growth method. *Chem. Mater. 15*, 1957−1962.
(44) Draine, B. T., and Flatau, P. J. (1994) Discrete-dipole approximation for scattering calculations. *J. Opt. Soc. Am. A 11*, 1491−1499.
(45) Johnson, P. B., and Christy, R. W. (1972) Optical constants of the noble metals. *Phys. Rev. B 6*, 4370−4379.

DOI: 10.1021/acs.bioconjchem.7b00427
Bioconjugate Chem. 2017, 28, 2452−2460